Corrections to the sixth-order anomalous magnetic moment of the muon

Clyde Chlouber and Mark A. Samuel
Quantum Theoretical Research Group, Department of Physics, Oklahoma State University, Stillwater, Oklahoma 74074
(Received 15 April 1977)

The contribution to the muon anomaly from fourth-order electron vacuum polarization is determined to order m_e/m_μ. The result, including the contribution from graphs containing two second-order lepton vacuum polarization subgraphs is $(\alpha/\pi)^3[(2/9)\ln^2(m_\mu/m_e)+(403/108-4\pi^2/9)\ln(m_\mu/m_e)+\zeta(3)/2+2\pi^2/27+5/27-6.56m_e/m_\mu]$.

In contribution to the muon anomaly from a vacuum polarization insertion G into a muon vertex diagram (Fig. 1) is given by[1]

$$a_\mu^G=\frac{\alpha}{\pi}\int_0^\infty\frac{dt}{t}\,\frac{\mathrm{Im}\pi^{(G)}(t)}{\pi}K_\mu^{(2)}(t)\,,$$

where

$$K_\mu^{(2)}(t)=\int_0^1 dx\,\frac{x^2(1-x)}{x^2+(t/m_\mu^2)(1-x)}. \tag{1}$$

Using the dispersion relation

$$\frac{\mathrm{Re}\pi^G(p^2)}{p^2}=\int_0^\infty\frac{dt}{t}\,\frac{\mathrm{Im}\pi^G(t)}{t-p^2}\,, \tag{2}$$

we can write the contribution in the form

$$a_\mu^G=-\frac{\alpha}{\pi}\int_0^1 dx(1-x)\mathrm{Re}\pi^G\left(p^2=\frac{-x^2}{1-x}m_\mu^2\right). \tag{3}$$

For fourth-order vacuum polarization insertions, the real and imaginary parts of the vacuum polarization kernel are known from the work of Källén and Sabry.[2] As shown by Lautrup and de Rafael,[1] the contribution from the proper diagrams (a), (b), (c) of Fig. 2 can be written as the following sum of terms:

$$\begin{aligned}I&=\frac{\mathrm{Im}\pi^{*(4)}(t)}{\pi}\int_{4m_e^2}^\infty\frac{dt}{t}K_\mu^{(2)}(t)\\&\quad+K_\mu^{(2)}(0)\int_{4m_e^2}^\infty\frac{dt}{t}\left[\frac{\mathrm{Im}\pi^{*(4)}(t)-\mathrm{Im}\pi^{*(4)}(\infty)}{\pi}\right]+R\\&=Q+R+S+\text{higher-order terms}\,,\end{aligned}$$

where

$$\begin{aligned}Q&=\tfrac{1}{4}\ln\frac{m_\mu}{m_e}+\frac{\zeta(3)}{2}-\tfrac{5}{12}\,,\\R&=\int_{4m_e^2}^\infty\frac{dt}{t}\left[\frac{\mathrm{Im}\pi^{*(4)}(t)-\mathrm{Im}\pi^{*(4)}(\infty)}{\pi}\right]\\&\qquad\times[K_\mu^{(2)}(t)-K_\mu^{(2)}(0)]\,,\\S&=-\frac{\mathrm{Im}\pi^{*(4)}(\infty)}{\pi}\int_0^{4m_e^2}\frac{dt}{t}[K_\mu^{(2)}(t)-K_\mu^{(2)}(0)]\,,\end{aligned} \tag{4}$$

and $\mathrm{Im}\pi^{*(4)}(t)/\pi$ is the contribution to the spectral function from the proper diagrams. The terms R and S are $O(m_e/m_\mu)$. We can easily extract the m_e/m_μ coefficient from S by using the asymptotic expansion[1] for $K_\mu^{(2)}(t)$:

$$K_\mu^{(2)}(t)=\left(\frac{\alpha}{\pi}\right)[\tfrac{1}{2}-\pi\sqrt{\tau}-4\tau\ln4\tau-2\tau+O(\tau^{3/2})]\,, \tag{5}$$

as $\tau=\dfrac{t}{4m_\mu^2}\to0$.

We find

$$S=\left(\frac{\alpha}{\pi}\right)^3\left[\frac{\pi}{2}\frac{m_e}{m_\mu}+O\left(\left(\frac{m_e}{m_\mu}\right)^2\ln\frac{m_\mu}{m_e}\right)\right]. \tag{6}$$

We now extract the coefficient of m_e/m_μ from R.

Upon making the change of variables $t=4m_e^2/(1-\delta^2)$, we obtain R in the form

$$\begin{aligned}R=\int_0^1\frac{2\delta d\delta}{1-\delta^2}&\left[\frac{\mathrm{Im}\pi^{*(4)}(t)}{\pi}-\tfrac{1}{4}\left(\frac{\alpha}{\pi}\right)^2\right]\\&\times\left[K_\mu^{(2)}(t)-\frac{\alpha}{2\pi}\right],\end{aligned} \tag{7}$$

where the substitutions

$$\frac{\mathrm{Im}\pi^{*(4)}(\infty)}{\pi}=\tfrac{1}{4}\left(\frac{\alpha}{\pi}\right)^2$$

and

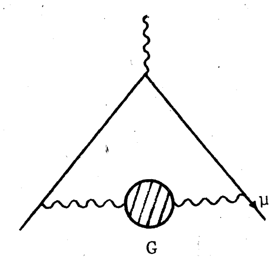

FIG. 1. Contribution to muon anomaly from vacuum polarization insertion into vertex diagram.

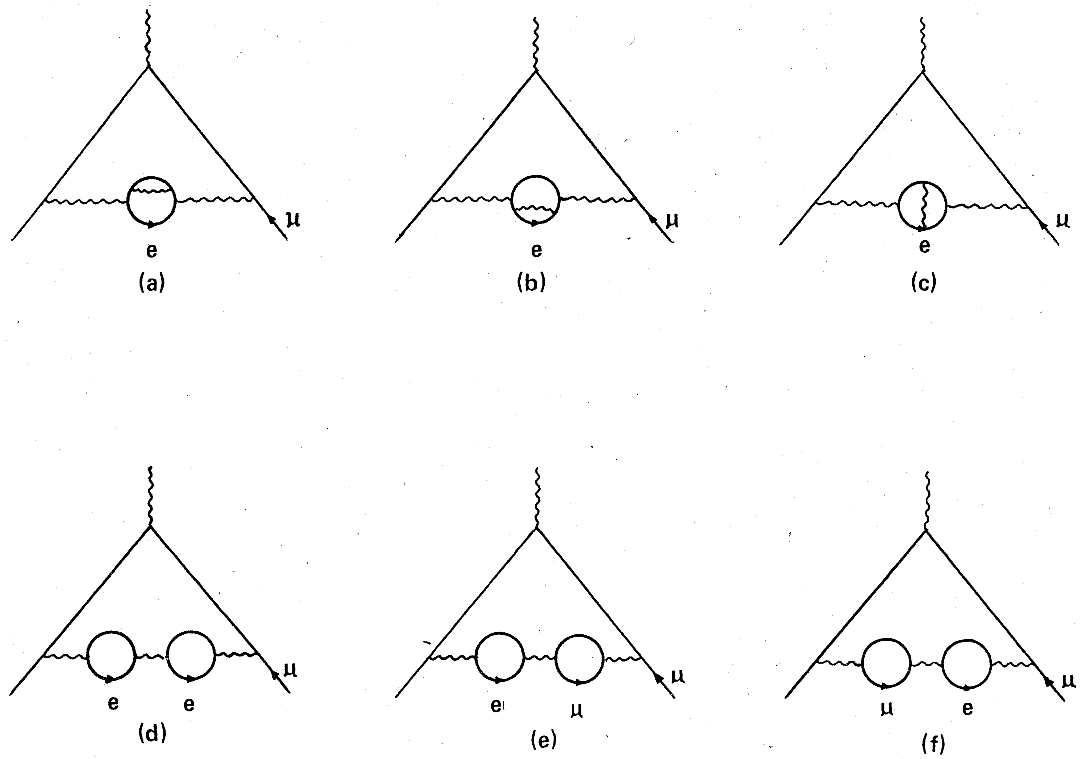

FIG. 2. Feynman diagrams representing the fourth-order vacuum polarization contribution to the sixth-order anomaly.

$$K_\mu^{(2)}(0)=\frac{\alpha}{2\pi}$$

have also been made. The coefficient of m_e/m_μ is

$$\lim_{m_e/m_\mu\to 0}\left(\frac{m_\mu}{m_e}R\right).$$

Making use of the analytic expression[1] for $K_\mu^{(2)}(t)$ valid for $0\leqslant t\leqslant 4m_\mu^2$,

$$K_\mu^{(2)}(t)=\frac{\alpha}{\pi}\left[\tfrac{1}{2}-4\tau-4\tau(1-2\tau)\ln 4\tau -2(1-8\tau+8\tau^2)\left(\frac{\tau}{1-\tau}\right)^{1/2}\cos^{-1}\sqrt{\tau}\,\right], \tag{8}$$

where

$$\tau=\frac{(m_e/m_\mu)^2}{1-\delta^2},$$

we obtain

$$\lim_{m_e/m_\mu\to 0}\left[\frac{m_\mu}{m_e}\left(K_\mu^{(2)}(t)-\frac{\alpha}{2\pi}\right)\right]=\left(\frac{\alpha}{\pi}\right)\frac{-\pi}{(1-\delta^2)^{1/2}}, \tag{9}$$

which gives the coefficient of m_e/m_μ from the R term:

$$\left(\frac{\alpha}{\pi}\right)^3 C_R=\lim_{m_e/m_\mu\to 0}\frac{m_\mu}{m_e}R = -2a\int_0^1\frac{\delta\,d\delta}{(1-\delta^2)^{3/2}} \times\left[\frac{\mathrm{Im}\,\pi^{*(4)}(t)}{\pi}-\frac{1}{4}\left(\frac{\alpha}{\pi}\right)^2\right]. \tag{10}$$

Although the integral for C_R could be evaluated analytically, an accurate numerical result is sufficient. We will use a geometric interval method with Padé approximants (type II) for accelerating the convergence of a sequence of Gauss quadrature approximations.[3,4] To verify that the method is applicable we must examine

$$\lim_{\epsilon_k\to 0}\frac{U_{k+m}}{U_k},$$

where $U_k=C(0,1-\epsilon_{k+1})-C(0,1-\epsilon_k)$ and the variables in C refer to the integration limits in Eq. (10):

$$C_R(0,1)=C_R.$$

Setting $\epsilon_{k+1}=r\epsilon_k$ with $0<r<1$ and $0<\epsilon_k<1$, we easily determine that

$$\lim_{\epsilon_k\to 0}\frac{U_{k+m}}{U_k}=(\sqrt{r}\,)^m.$$

TABLE I. Sequence of quadrature approximations S_k to C_R is shown along with differences U_k and ratios U_{k+1}/U_k.

k	S_k	$S_{k+1}-S_k$	U_{k+1}/U_k
1	−7.073 097 930 873	−0.051 185 228 598 83	0.709 074 551
2	−7.124 283 159 471	−0.036 294 143 019 98	0.708 205 255
3	−7.160 577 302 491	−0.025 703 702 841 63	0.707 713 914
4	−7.186 281 005 333	−0.018 190 868 160 58	0.707 439 481
5	−7.204 471 873 494	−0.012 868 938 339 89	0.707 287 760
6	−7.217 340 811 834	−0.009 102 042 578 740	0.707 204 596
7	−7.226 442 854 412	−0.006 437 006 351 021	
8	−7.232 879 860 763		

Choosing $r=\frac{1}{2}$ corresponds to doubling the number of quadratures from one approximation to the next. The interval $\{0, 1\}$ is divided into 2^{k-1} equal subintervals. An eight-point Gauss quadrature is then applied to each subinterval. The partial sums S_k of the numerical quadratures are shown in column II of Table I. The results of column IV of Table I indicate that the ratios U_{k+1}/U_k are indeed approaching $1/\sqrt{2}$ as k increases:

$$U_k = S_{k+1} - S_k \,.$$

The first three Padé approximants to the sequence S_k are

$$S^{\{N,N\}}(0) = \begin{cases} -7.248\,293\,852\,862\,7\,, & N=1 \\ -7.248\,420\,797\,243\,5\,, & N=2 \\ -7.248\,421\,968\,554\,8\,, & N=3\,. \end{cases}$$

We combine the $\{3, 3\}$ estimate for C_R with the coefficient of m_e/m_μ from S to obtain

$$\left(\frac{\pi}{2} - 7.24842\right)\frac{m_e}{m_\mu} = -5.677\frac{m_e}{m_\mu}\,. \qquad (11)$$

As an independent check on this result and also an additional check on our routine VAC4[3] we computed numerically

$$I\left(\frac{m_e}{m_\mu}\right) = -\frac{\alpha}{\pi}\int_0^1 dx(1-x)\left\{\mathrm{Re}\,\pi^{(4)}\left(\frac{-x^2}{1-x}m_\mu^2\right) + \left[\mathrm{Re}\,\pi^{(2)}\left(\frac{-x^2}{1-x}m_\mu^2\right)\right]^2\right\} \qquad (12)$$

as a function of m_e/m_μ. The results, $Q(m_e/m_\mu) - I(m_e/m_\mu)$, along with those for the direct numerical evaluation of $R(m_e/m_\mu)+S(m_e/m_\mu)$ from Eqs. (4), are shown in Table II and plotted in Fig. 3. The results in the figure are seen to be consistent with a curve that is asymptotic to a line passing through the origin with slope 5.68. Finally, we consider the contribution from the double-bubble diagram[5] [Fig. 2(d)],

TABLE II. $Q-I$ and $R+S$ are computed numerically as a function of the mass ratio. The asterisk denotes the physical mass ratio case.

	$10^4\frac{m_e}{m_\mu}$	$10^3\left[Q\left(\frac{m_e}{m_\mu}\right)-I\left(\frac{m_e}{m_\mu}\right)\right]$	$10^3(R+S)$
1	4.396 66	2.430 285	2.425 92
2	8.793 32	4.972 909	4.768 81
3	13.189 99	7.150 836	7.046 65
4	17.586 66	9.284 515	9.268 54
5	21.983 32	11.416 20	11.440 55
6	26.379 99	13.532 35	13.567 17
7	30.776 65	15.614 07	15.651 95
8	35.173 32	17.665 35	17.697 79
9	39.569 96	19.675 72	19.707 09
10	43.966 62	21.651 24	21.681 95
*11	48.363 28	23.590 54	23.624 17

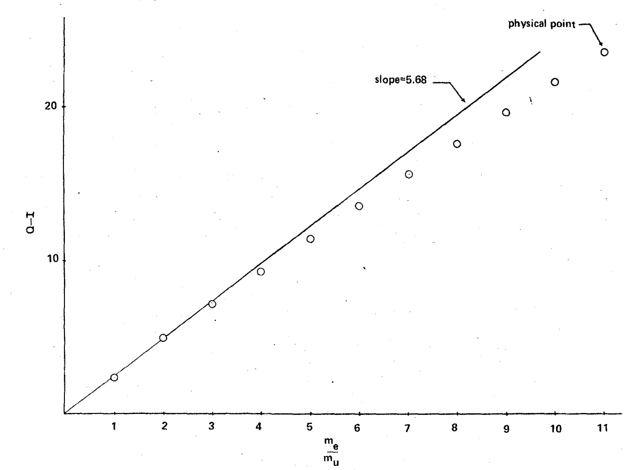

FIG. 3. Fourth-order vacuum polarization contribution to $a_\mu^{(6)}$ (proper diagrams) from terms of $O(m_e/m_\mu)$. The units for the abscissa and ordinate are 4.396 66 $\times 10^{-4}$ [physical $(m_e/m_\mu)/11$] and $10^{-3}(\alpha/\pi)^3$, respectively.

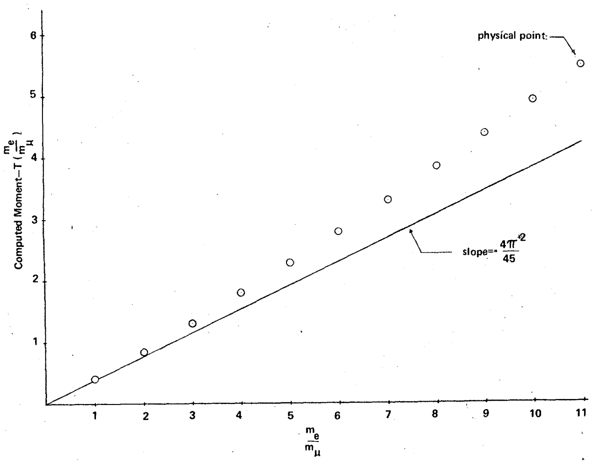

FIG. 4. Double-bubble contribution to $a_\mu^{(6)}$ from terms of $O(m_e/m_\mu)$. The analytic value $T(m_e/m_\mu)$ is given in Eq. (13). The computed moment is evaluated from the second term of Eq. (12). Units are the same as for Fig. 3.

$$\left(\frac{\alpha}{\pi}\right)^3\left\{\left[T\left(\frac{m_e}{m_\mu}\right)=\left(\tfrac{2}{9}\ln^2\frac{m_\mu}{m_e}-\tfrac{25}{27}\ln\frac{m_\mu}{m_e}+\tfrac{317}{324}+\frac{\pi^2}{27}\right)\right] -\frac{4\pi^2}{45}\frac{m_e}{m_\mu}\right\}. \tag{13}$$

This contribution has been determined with sufficient accuracy to verify the $O(m_e/m_\mu)$ term, as well as to determine the next term, which is approximately $2(m_e/m_\mu)^2\ln^2(m_\mu/m_e)$. The results are shown in Fig. 4. Taking this into account, as well as the leading contribution Q from the proper diagrams, and the contribution of the mixed diagrams [Figs. 2(e) and 2(f)] we finally determine the contribution to the muon anomaly from all the diagrams of Fig. 2 to be

$$\left(\frac{\alpha}{\pi}\right)^3\left[\tfrac{2}{9}\ln^2\frac{m_\mu}{m_e}+\left(\tfrac{403}{108}-\frac{4\pi^2}{9}\right)\ln\frac{m_\mu}{m_e} +\frac{\zeta(3)}{2}+\frac{2\pi^2}{27}+\tfrac{5}{27}-6.56\frac{m_e}{m_\mu}\right]. \tag{14}$$

For the mixed lepton double-bubble diagrams [Figs. 2(e) and 2(f)], it was explicitly verified that there is no $O(m_e/m_\mu)$ term. [The remainder goes as $(m_e/m_\mu)^2$.]

In summary, our numerical result [including terms of $O(m_e/m_\mu)$ and smaller] changes the contribution of these graphs by

$$-0.0291\left(\frac{\alpha}{\pi}\right)^3=-0.36\times10^{-9}(-4\text{ ppm}).$$

This work was supported by the U.S. Energy Research and Development Administration.

[1]B. E. Lautrup and E. de Rafael, Phys. Rev. 174, 1835 (1968).
[2]G. Källén and A. Sabry, K. Dan. Vidensk. Selsk. Mat. Fys. Medd. 29, No. 17 (1955).
[3]C. Chlouber and M. A. Samuel, Comput. Phys. Commun. (to be published).
[4]The coordinates are chosen to be $S_{k+1}-S_k$.
[5]M. A. Samuel, Nucl. Phys. B70, 351 (1974).